Experiments in Fluids manuscript No.
(will be inserted by the editor)

Laser Marked Shadowgraphy: a novel optical planar technique for the study of microbubbles and droplets

S. Dehaeck · H. Van Parys · A. Hubin · J.P.A.J. van Beeck

Received: date / Accepted: date

Abstract A novel combination of backlighting and Glare Point Velocimetry and Sizing (GPVS) is proposed to measure the size distribution of microbubbles (or microdroplets). This new technique, which we will call Laser Marked Shadowgraphy or LMS, avoids sizing out-of-focus bubbles (or droplets) and the associated bias error. Compared to backlighting, this combination also improves the precision of the diameter measurement and allows void fraction measurements. Compared with GPVS, a more robust image processing is obtained. The applicability of the developed technique is demonstrated on a cloud of electrochemically generated hydrogen bubbles.

Keywords LMS, Backlighting, Shadowgraphy, Glare Points, Droplets, Electrochemistry, Hydrogen Bubbles, Sizing, GPVS, Inverted Rotating Disk Electrode

1 Introduction

Many industrial processes deal with gas bubbles, e.g. the production of ammonia, waste water treatment or electrochemical processes such as the electro-winning of metals, the production of chlorine, etc. In terms of reactor design and optimization, it is necessary to describe the influence of the gas bubbles on the fluid flow and mass transport in a

This research was funded with fellowship SB-031241 and SBO contract number 040092 granted by the Institute for the Promotion of Innovation through Science and Technology in Flanders (IWT-Vlaanderen).

S. Dehaeck, J.P.A.J. van Beeck

Von Karman Institute for Fluid Dynamics, Waterloose Steenweg 72, B-1640 Sint-Genesius-Rode, Belgium

S. Dehaeck (Current Address)

University Libre de Bruxelles, Transfers, Interfaces and Processes (TIPs) - Physics of Fluids, Av. F.D. Roosevelt 50, CP 165/67, B-1050 Brussels, Belgium

H. Van Parys, A. Hubin

Vrije Universiteit Brussel, Research Group Electrochemical and Surface Engineering, Pleinlaan 2, B-1050 Brussels, Belgium

E-mail: sam.dehaeck@gmail.com

quantitative way. Depending on the process conditions a large quantity of small bubbles can be produced. Therefore the need exists for a robust and accurate technique that can measure the bubble characteristics in situ and non-intrusively.

A typical choice for such measurements is backlighting or shadowgraphy. Here, the bubble is illuminated by a diffuse lightsource and its shadow is imaged. This technique is straightforward in the sense that it is unlikely that a circular shadow is visible in an image, which does not represent a bubble. This makes the technique robust as it will not pick up random dust particles. The main disadvantage of backlighting though is that the distance of the imaged bubbles to the camera is not known precisely. Any bubble between the light source and the camera will cast a shadow. Thus, out-of-focus bubbles inevitably appear in the image. Sizing these bubbles can lead to considerable sizing errors as will be shown experimentally. This 'defocus bias' was also demonstrated by e.g. Ren et al. (1996) where sizing errors of up to 100% were found for small bubbles. Another disadvantage of this unkwown distance to the camera is that void fraction measurements are inaccurate because the measurement volume is not well-defined.

Glare Point Velocimetry and Sizing, as introduced by Dehaeck et al. (2005), is another 2D optical measurement technique capable of measuring (spherical) bubble diameter distributions non-intrusively. Here, the bubble is illuminated from two sides with a laser beam and the camera is placed at a scattering angle of 90° with respect to either beam. In this symmetrical configuration, two externally reflected glare points are visible on either side of the bubble. From the distance between these glare points, the bubble diameter can be calculated with a precision which is an order of magnitude more precise (Dehaeck et al. (2005)). Additionally, as only bubbles inside the thin laser-sheet are sized, the measurement volume is well-defined. As a result, both of the mentioned disadvantages of backlighting, i.e. defocus bias and inaccurate void fraction measurements, are not prominently present in GPVS. However, the processing of the images is less robust than for backlighting. A bubble with GPVS is only represented by two glare points, which are e.g. on the same pixel row. Now, when the amount of bubbles in the image is sufficiently large, spurious glare points will appear on the bubble surface, coming from laserlight which has been scattered by other bubbles. These extra glare points could easily be paired with other glare points to create 'imaginary' bubbles. Thus, the 'signature' of a bubble is not strong enough with GPVS and this is precisely where backlighting excels.

To overcome these drawbacks, a combination of both techniques, which we will call Laser Marked Shadowgraphy (LMS), is advisable. The first step in this direction was taken by Haines and Johnson (1995) who used two narrow light-sheets, perpendicular to the optical axis and opposing each other, to limit the measurement volume of regular backlighting. Bubbles inside these light-sheets reflected light towards the camera which was visible as differently coloured glare points inside the bubble contour. Thus, by sizing only those shadow contours with coloured glare points, one could avoid sizing out-of-focus bubbles (provided the light sheets were sufficiciently thin).

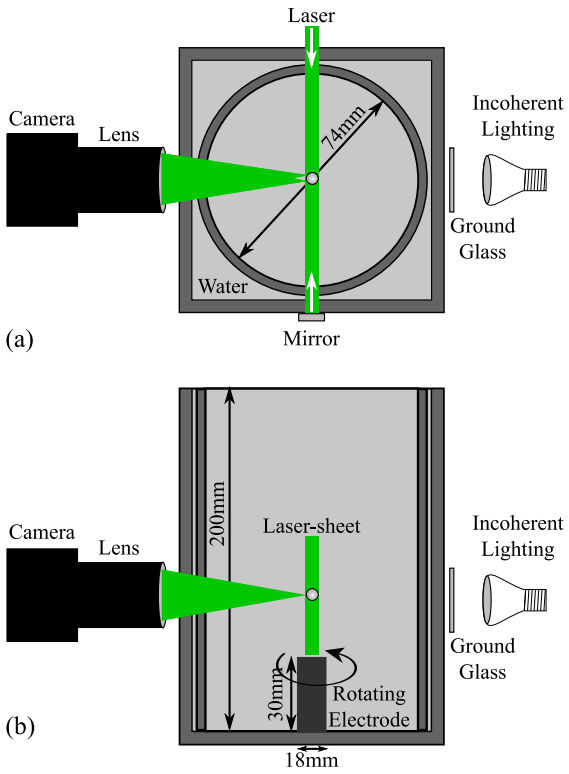

Fig. 1 (a) Top view of the iRDE. (b) Side view of the iRDE.

However, Haines and Johnson (1995) did not use the glare point theory and as was shown by Dehaeck et al. (2005), this could improve the sizing precision of the bubble when based on the distance between two glare points. Thus, a spherical bubble sizing technique will be presented in this article that obtains the accuracy and precision of GPVS while keeping the robust image processing of backlighting. This technique can also be applied without modification to measure spherical droplets or (specularly reflecting) opaque particles.

After an explanation of the experimental set-up in section 2, a hydrogen bubble will be analysed to demonstrate the image processing algorithm in section 3. Section 4 then determines the defocus bias error of regular backlighting on sample pictures. Finally, as a validation of the LMS technique in a demanding experimental set-up, experiments are carried out in section 5 on electrochemically generated bubbles formed in an inverted rotating disc electrode (IRDE). The resulting bubble size distributions were calculated and analysed for both stagnant and rotating flow, showing the experimental relevance of the technique.

2 Experimental Set-Up

A sketch of the top and side view of the experimental set-up is shown in figure 1(a) and (b) respectively. It is a combination of backlighting with a 1000W halogen light source (and a ground glass to increase the diffusivity of the illumination) and a GPVS set-up where the continuous Argon ion laser sheet (and its reflection) crosses the test section perpendicularly

to the optical axis of the lens. Now, as the hydrogen bubbles in general are of the order of 100μm (Wedin et al. (2003) and Boissonneau and Byrne (2000)), a high magnification lens is required to image the bubbles on a sufficient amount of pixels. To this end, a 16X Precision Zoom Lens from Edmund Optics was chosen (with a maximum optical magnification of 12) which required a stand-off distance of 5.6cm. The used digital camera was a Pixelfly 12bit greyscale camera.

Electrochemical measurements are performed with a three electrode configuration using a potentiostat PGSTAT12® controlled by the GPES 4.8 software. The working electrode consists of a small platinum disk (4mm diameter, Alfa Aesar, 99.99% purity) embedded in the top surface of a PVDF cylinder (18mm diameter). The counter electrode is a large platinum grid and the reference electrode is a Ag/AgCl (saturated KCl) electrode (Schott-Geräte)). This 3-electrode system enables us to control the potential and current of the working electrode. For the preparation of the solutions once-distilled and demineralized water and analytical reagents (all Merck p.a.) are used. As a case study, the formation of hydrogen bubbles in 0.1M Na_2SO_4 is studied at -1.7V vs Ag/AgCl sat. The pH of the solution is fixed at 1.5 by adding concentrated sulphuric acid (H_2SO_4) to the solution. Partly due to the heating of the electrolyte by the 1000W halogen light source, a water jacket controlled by a thermostat (Lauda 304) is used to keep the temperature of the electrolyte constant at 25$\pm$0.1°C.

3 Image Processing

The bubbles under study are hydrogen bubbles which are electrochemically generated, according to reaction 1, by cathodically polarising the working electrode.

$$2H^+ + 2e^- \rightarrow H_2(gas) \tag{1}$$

A picture of such a single in-focus hydrogen bubble is shown in figure 2(a). In this section, this image will be analysed with Laser Marked Shadowgraphy (LMS) in two steps. First, a restricted search for glare points is performed (to avoid sizing out-of-focus bubbles) and secondly, the sizing precision is improved by calculating the bubble diameter from the inter glare point distance.

On figure 2(a), one notices the circular shadow, coming from regular backlighting, and the white points (i.e. glare points) inside this contour, coming from reflection of the two laser-sheets. Now, the presence of glare points marks that this particular bubble is located in the thin measurement volume defined by the laser-sheet. Note however that only the two points at the same height as the centre of the bubble and close to the shadow edge are coming from direct reflection of the original and the reflected laser-sheet. The other glare points visible in the lower left quadrant are scattering light that has already been deviated by other bubbles. Therefore, the presence of these extra glare points is no strict guarantee that the bubble is inside the laser-sheet and, as such, should not be taken into account.

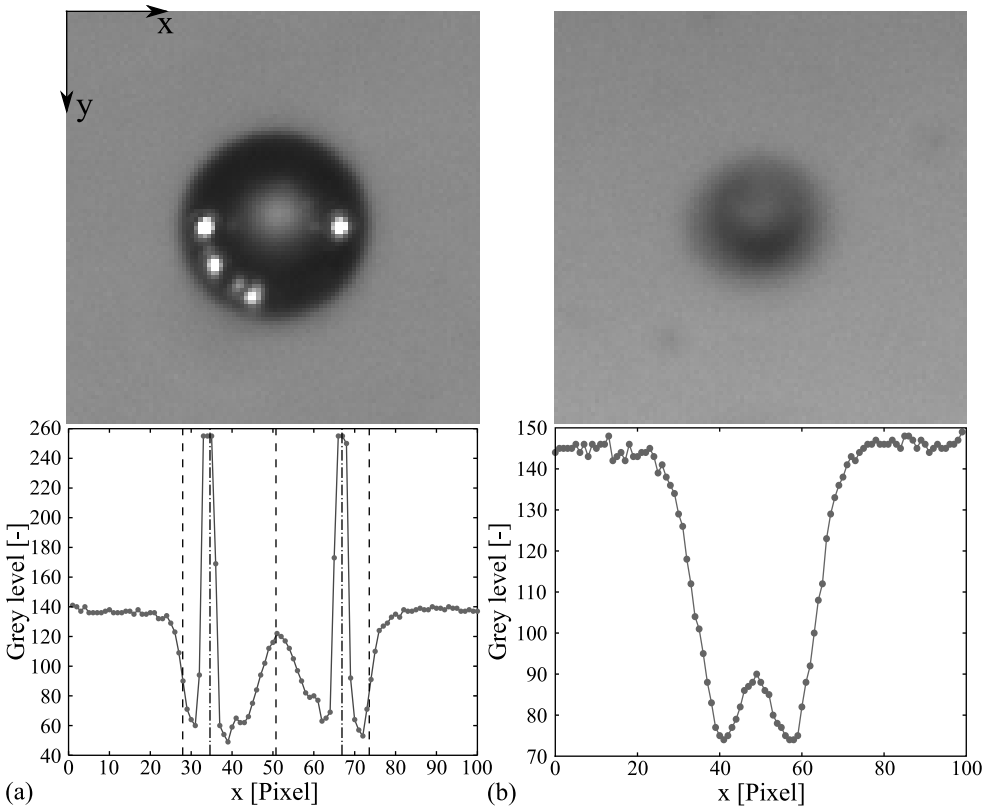

Fig. 2 Intensity versus column plot for the central row (a) for an in-focus bubble with glare points and (b) for an out-focus bubble without glare points.

One possible automated processing scheme to detect and size this bubble, is to start with a circle detection algorithm that is capable of detecting black discs in an image as e.g. the Circle Hough transform (e.g. Minor and Sklansky (1981)), the Gradient Pair Method that is used in the present work (Rad et al. (2003)) or the curvature-profile method proposed in Pla (1996) and Honkanen et al. (2005). Once the bubble is detected, a check for the presence of the two (correct) glare points is performed. This check should allow to discriminate against glare points coming from multiple scattering and therefore a restricted search area inside the contour is necessary. This is possible as the position of the glare points can be calculated from the estimated bubble centre location C_x and diameter D_b (both in pixel) obtained from the circle detection algorithm through the formula derived from basic trigonometry:

$$GP_x = C_x \pm \frac{D_b}{2\sqrt{2}} \tag{2}$$

with the x- and y-axis defined in the figure and GP_x the x-location of the glare points in pixel. The y-location of the glare point for the present configuration is the same as the y-location of the shadow centre. To explain this step on an example, a horizontal intensity profile through the centre of the shown bubble (and through both glare points) is plotted in figure 2(a). The vertical dashed lines present in this figure indicate the bubble centre and its edges as obtained from the circle detection (and sizing) program. Now, from this estimated bubble centre position and diameter, the expected

glare point locations were calculated from equation 2 and indicated on the profile in dash-dot lines. Checking for the presence of glare points at the specified locations can be based on the intensity level at the calculated position. Because the reflected glare points can be made more intense than the backlighting illumination level, a simple check whether the intensity at the predicted location is above the average backlighting signal is enough to validate the bubble as being inside the laser-sheet. This multiple intensity level approach is similar to the work of Lindken and Merzkirch (2002) where backlighting and Particle Image Velocimetry data were separated in the same way. Now, it is clear that this restricted search for glare points will not validate the glare points coming from multiple reflections visible in the lower left quadrant of figure 2. However, these spurious glare points are no definitive proof that the imaged bubble is in the laser defined measurement volume. In figure 2(b) an out-of-focus bubble is shown. In this case, the transient is spread over more pixels and estimating the correct location of the bubble edge becomes even more uncertain as explained in Bongiovanni et al. (1997).

However, there is more information present in the picture which we can use to our benefit. When both glare points are present and the bubble is spherical, the bubble diameter D_b can be inferred from the separating distance of these glare points at 90° as follows (c.f. Dehaeck et al. (2005)):

$$D_b = \sqrt{2} C \delta_{pix} \tag{3}$$

where δ_{pix} is the separating distance in pixels between the glare points and C is the number of millimetres per pixel (i.e. the calibration constant). Applied to figure 2, the difference between the diameter obtained with backlighting and the one with GPVS is only 0.2%. Note that this difference is no statistical average but only an illustration on this particular bubble.

However, the estimate from GPVS is not only useful as a redundant measurement of the bubble diameter (and location), it is also more precise. This is because the glare points can be fitted with a Gaussian to obtain their position with sub-pixel accuracy. As was proven theoretically by Bongiovanni et al. (1997), such a fitting procedure is not possible with regular backlighting. This implies that the 'real' bubble edge can be located almost anywhere in the transitional region where the pixel intensity changes from black to white. Thus, the uncertainty on the measured diameter with backlighting depends on the amount of diffraction in the optical setup. For the intensity profile shown in figure 2(a), an uncertainty of ± 2 pixel on the shadow diameter estimation is a reasonable estimate as each dashed line can easily be shifted by a single pixel and remain in the transient region. While this estimate is not a statistical value, its value is a direct consequence of the study of Bongiovanni et al. (1997). In contrast, the sharp intensity peaks of GPVS can be fitted with a Gaussian. The uncertainty on estimating the distance between two Gaussian fitted intensity peaks was statistically investigated for different intensity and noise levels by Marxen et al. (2000) for a different measurement technique called Particle Tracking

Velocimetry and therefore such experiments were not repeated here. They found that this uncertainty is of the order of 0.1 pixel. Assuming that the presence of a backlighting signal does not modify this uncertainty, this value can be used as input for an estimation of the bubble sizing uncertainty in LMS, we obtain $0.1/(D_{pix}/\sqrt{2})$ (with D_{pix} the bubble diameter expressed in pixels and $D_{pix}/\sqrt{2}$ the distance between the two glare points). This can be compared with the estimate for backlighting: $2/D_{pix}$. Thus, taking the ratio of these two relative uncertainties to find the improvement, one obtains as an order of magnitude estimate that LMS outperforms backlighting by a factor $10\sqrt{2}$.

Note that this improvement on the relative uncertainty does not depend on the bubble image size. Nevertheless, there is a secondary effect that does depend on the bubble size. With LMS a large dynamic range of bubbles can be measured. The smallest bubble image size is determined by the need to separate the two glare points by several pixels leading to a minimum bubble diameter of roughly 10 pixels. The largest bubble image size only needs to fit on the sensor, i.e. have a diameter smaller than 1000 pixels. Thus, the dynamic range equals 100. Yet, as the reflected intensity scales with the diameter squared, this implies that the glare point intensity varies with a factor 10000. This is far greater than any current camera can capture and saturation of the camera will inevitably follow. This saturation of the glare points will render the fitting with a Gaussian less accurate, which decreases the relative improvement of GPVS over backlighting. In extreme cases where this might lead to a better uncertainty for regular backlighting, the advantage offered by avoiding the defocus bias by the twin glare points still offers an advantage of LMS over regular backlighting.

Finally, note that the use of a laser-sheet is not required for LMS; any parallel light-sheet (e.g. created by a normal light bulb and a parabolic mirror) will do. Additionally, the presence and the location of these externally reflected glare points is completely independent of the relative refractive index. Therefore, formulae 2 and 3 can be applied without modification to measure droplets and even opaque (but specularly reflecting) particles when two light-sheets are used.

4 Defocus Bias Errors

Going from a single bubble to multiple electrochemically generated hydrogen bubbles in figure 3, which is a typical picture obtained in the experimental set-up, one notes that many bubbles are backlit but only some of them have the twin glare points. Now, the basic principle of LMS (and the image processing scheme explained above) is that only the bubbles with the twin glare points are sized. Thus, the detection volume associated with LMS in the case of a laser with a top-hat intensity profile is illustrated in Figure 4. This shows that, for a top-hat intensity profile, the thickness of the measurement volume T_M is equal to the laser-sheet thickness T_L and independent of the bubble diameter. There is only a displacement of the detection volume with respect to the laser-sheet; more specifically, it is shifted away from the lens by a distance $R/\sqrt{2}$. For a Gaussian intensity profile of the laser-sheet, the thickness of the detection volume becomes dependent on

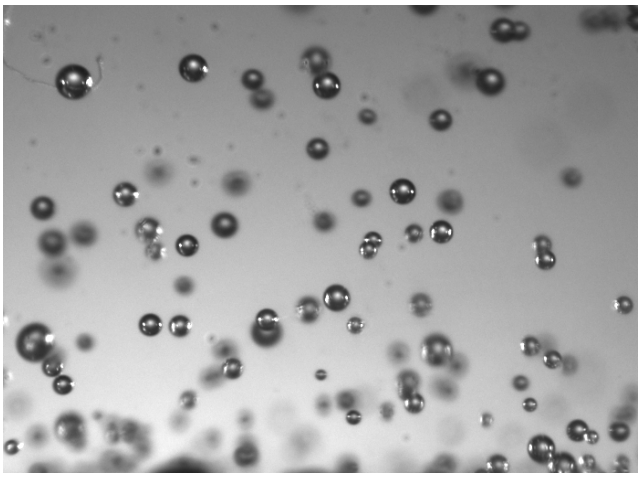

Fig. 3 Example image of LMS; only the bubbles with two symmetrical glare points are in-focus.

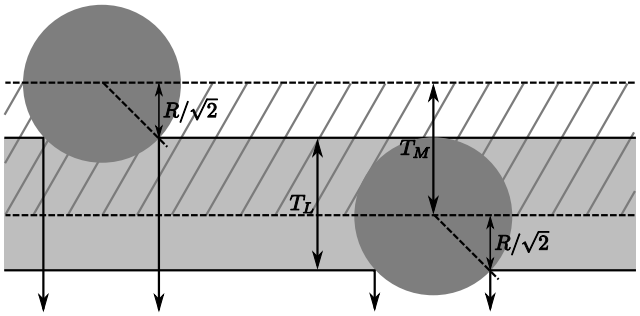

Fig. 4 Influence of laser-sheet thickness and bubble radius on the displacement of the detection volume.

the bubble radius as smaller bubbles need more incoming light to be able to reflect a visible glare point towards the camera and thus can only use the more intense central portion of the laser-sheet. Larger bubbles are visible in a larger portion of the laser-sheet. These phenomena become important when void fraction measurements are attempted where the bubble size approaches or exceeds the laser-sheet thickness. This effect has been studied extensively in PDA and we refer to Albrecht et al. (2003) for a more rigorous description. Correcting for the different measurement volumes for the different bubble sizes is important in order to estimate the void fraction in the flow. Another important error source for such measurements with increasing void fractions is the blocking of the incoming laser-sheet by the increasing number of bubbles, which will lead to the absence of glare points on in-focus bubbles. This will lead to an underestimation of the void fraction. On the contrary, this blocking is not expected to bias the diameter distribution measurements as the glare points on both large and small bubbles are shielded alike.

Bubbles located in the measurement volume are at a known distance to the camera (accurate up to the laser-sheet thickness). Bubbles without glare points can be located closer to or further away from the lens, either case leading to sizing errors, i.e. the defocus bias error. This error is caused both by the blurring of the image contour and by the dependency of the magnification on the distance of the bubble to the objective. This effect was investigated theoretically in Bongiovanni et al. (1997)) and experimentally by e.g. Ren et al. (1996). Therefore, no statistical analysis will be given

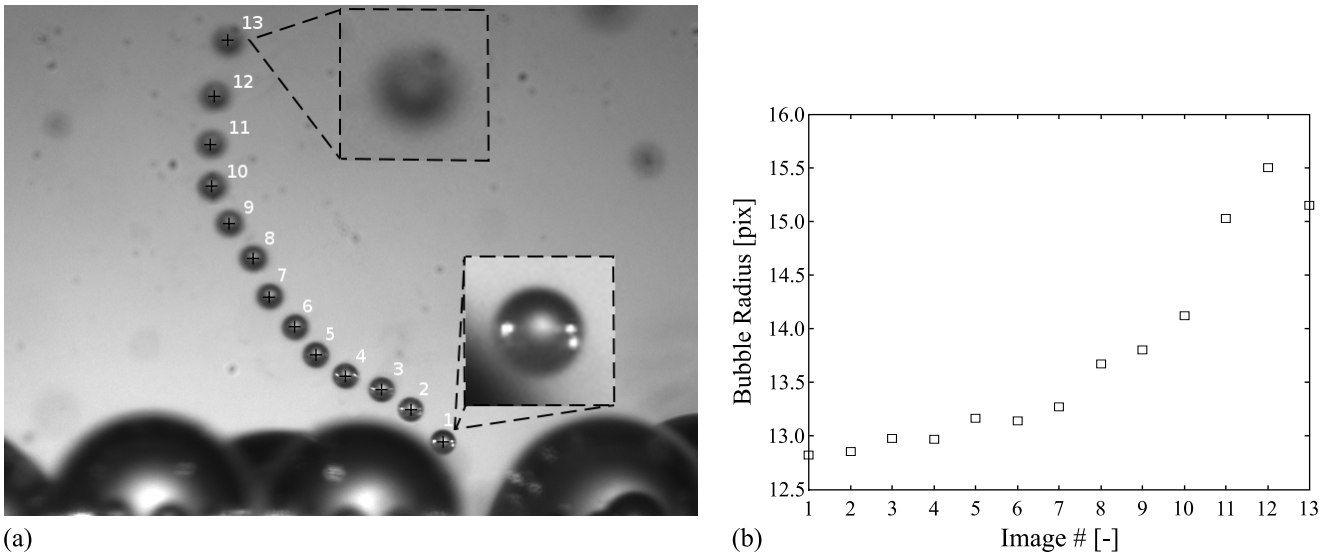

(a) (b)

Fig. 5 (a) Overlay of several images and the detected trajectory of a bubble rising and going out-of-focus (b) Evolution of measured shadow bubble size versus image number

here but the magnitude of this error will only be illustrated for our experimental set-up and the associated improvement of the suggested LMS technique.

To this end, the location and size of one bubble ($\pm$ 100μm) is tracked over multiple pictures as it rises and goes out-of-focus. An overlay of these pictures is shown in figure 5(a). The black crosses represent the detected positions of the bubble centre. Remark that there are large bubbles present at the bottom of the picture. These bubbles are artefacts of the used electrode design and are not investigated in this article. In this picture, one can clearly see that the bubble only has glare points in the first 4 images and then goes out-of-focus. Whether the bubble moves towards or away from the camera is impossible to say. The impact of this blurring on the measured bubble diameter with backlighting is shown in figure 5(b), where the measured radius (in pixels) is plotted versus the image number. This shows that blurring makes the bubble appear larger than it really is. This difference reaches up to 21% of the in-focus diameter in the present case. Note that with LMS only the first 4 images would be used for sizing, leading to a maximum difference of only 1.2% between the different results. Thus, with LMS one can limit the sizing error to 1.2% whereas regular backlighting could have a bias error of up to 20 times larger.

Buoyancy effects can certainly be neglected as the origin of the growing bubble size in figure 5 as it only rises 1.6mm in the shown image, which corresponds to a difference of 0.0052% in the radius. Nevertheless, one could still argue that the noticed increase in bubble size comes from the continued diffusion of hydrogen into the bubble. Figure 6 proves that this is not the case. Here, a bubble following a nearly horizontal path is followed from left to right. Faint glare points are only present in the first and last image of the sequence. While this is not visible in the shown magnifications, intensity plots do show weak peaks. Thus, the bubble goes out-of-focus and returns again. This is also seen in figure 6(b) where

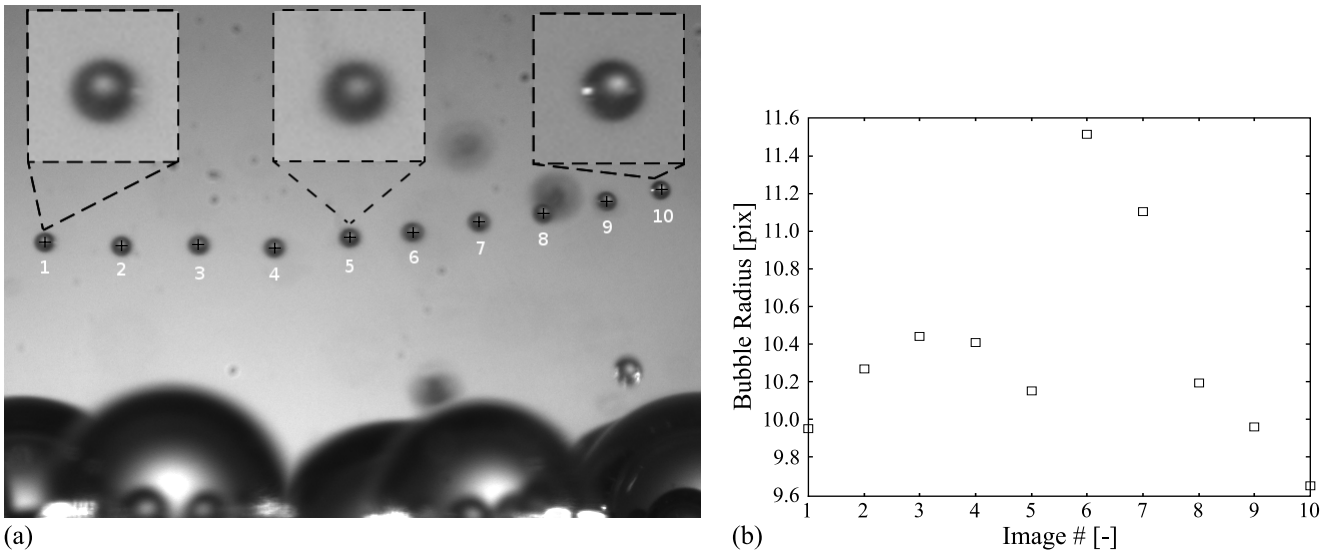

Fig. 6 (a) Overlay of several images and the detected trajectory of a bubble going from left to right (b) Evolution of measured shadow bubble size versus image number

the bubble radius is plotted versus the picture number. While the change between pictures is rather coarse due to the difficulty of measuring out-of-focus bubbles, a clear increase in radius is observed (up to 10%) followed by a decrease. This behaviour cannot be explained by other phenomena than by an enlargement due to out-of-focus blurring. Also note that the starting and ending value are similar as both are (nearly) in-focus.

The above examples show that the defocus bias error can reach high values in the present set-up. While this maximum error depends on the experimental settings and the processing algorithm, other authors (e.g. Ren et al. (1996) and Bongiovanni et al. (1997)) also obtained significant defocus errors, some even in excess of 100% (Ren et al. (1996)). In order to decrease this defocus bias, Ren et al. (1996) applied corrections to the obtained size estimate based on the contrast of the image. In this way, they reported that measurements of in- and out-of-focus bubbles were possible with an uncertainty below 10%. While the present technique does not allow sizing of out-of-focus bubbles, it does decrease the defocus bias error more effectively.

5 Application of the Technique

As both backlighting and GPVS have been calibrated previously, no calibration was deemed necessary for the combination of both techniques. Instead, the applicability of the LMS technique is shown in a demanding experimental measurement in the IRDE (Inverted Rotating Disc Electrode). This reactor is specially designed for the study of two-phase flows in a controlled way, as shown in Van Parys et al. (2007). The IRDE consists of a cylindrical vessel with a working electrode placed at the bottom of the cell. Hydrogen bubbles are generated at the working electrode, which can rotate around its axis. As a result, the formed bubbles can detach either by buoyancy or be swept away by the rotational

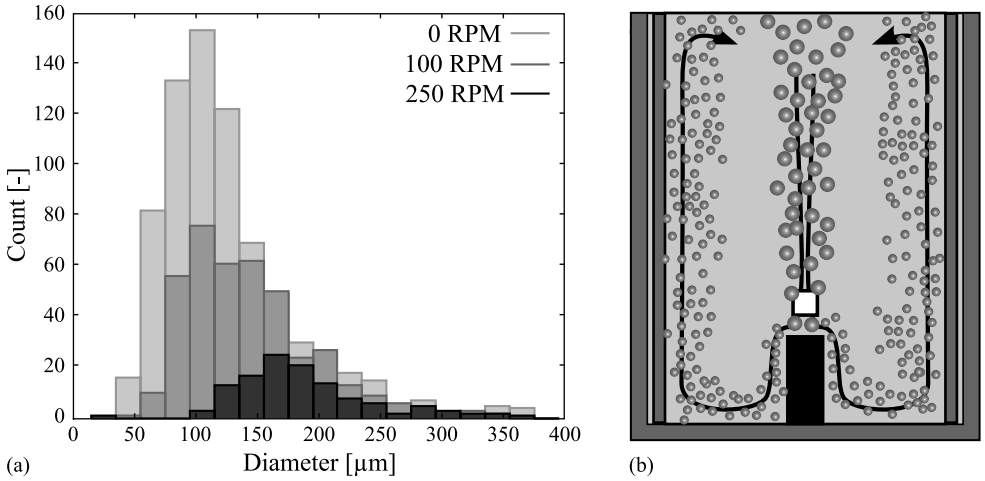

Fig. 7 (a) Diameter distributions for different rotational speeds and pH=1.5 (b) Expected flow behaviour in the inverted rotating disc electrode and the location of the measurement volume (white square).

movement of the electrode. The counter electrode is placed at the top of the cell. The reference electrode is placed in the solution from the top. In order to have an optimal optical access and to control the temperature inside the electrochemical cell, the cylindrical cell is placed in a rectangular box filled with water of which the temperature is controlled by means of a thermostat.

In a first step, an electrochemically formed bubble plume in stagnant flow is investigated (0 rpm). Figure 7(a) shows the diameter distribution of hydrogen bubbles in a stagnant flow. It is a standard log-normal distribution with a mean bubble diameter of 115 μm. This agrees with values found in literature (Wedin et al. (2003) and Boissonneau and Byrne (2000)), where the diameter of hydrogen bubbles ranged from about 45 μm to 200 μm.

In a next step, the influence of the rotational speed of the working electrode on the bubble size diameter some millimeters above the electrode is studied. Figure 8 shows the average bubble diameter as a function of rotational speed. This was repeated in three independent experiments so as to demonstrate the repeatability of the measurements. From this plot, a clear increase in bubble size with the rotational speed is observed in the measurement point above the electrode. Looking at the obtained diameter distributions in figure 7(a), a shift towards larger diameters is indeed noticeable. However, when looking closer, one notices that the total amount of bubbles has decreased significantly, as the ordinate of this figure is the total count of bubbles of a certain size range over a constant time (approximately 90 seconds). Given that the total amount of produced gas is not expected to decrease at higher rotational speeds, a large part of the produced gas must go somewhere else. This is indeed very plausible when looking at the expected flow behaviour in figure 7(b) and the position of the measurement volume directly above the electrode. Due to the rotation of the electrode, large vortices will appear. This creates a downward flow in the centre of the cell, which will counter the bubble plume rising from the electrode. As a result, only the largest bubbles with the most buoyancy will be able to rise to the surface. Smaller

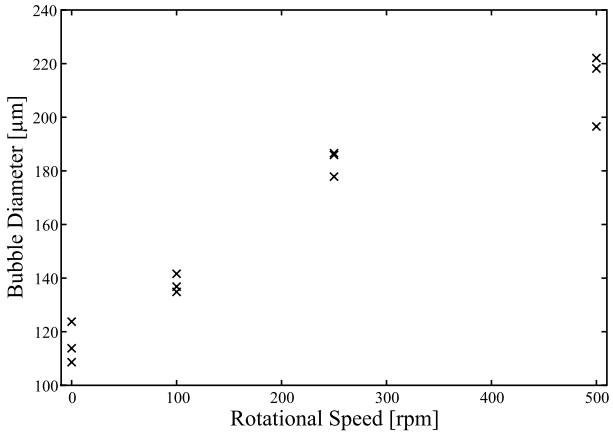

Fig. 8 Average bubble diameter versus rotational speed in the iRDE for three independent experiments.

bubbles will be swept away with the flow and hence will not pass the measuring volume. This hypothesis was confirmed by preliminary visualisation experiments, which are not shown here. Returning to 7(a), it is clear that many of the bubbles smaller than 100μm are no longer detected at a rotational speed of 100 rpm and are completely gone for 250 rpm, whereas the amount of bubbles of 300μm remains approximately the same for the three different rotational speeds.

Note however that this result does not imply that the average bubble diameter created at the electrode surface increases with rotational speed. To examine this dependency, further measurements are necessary at other locations in the IRDE so as to obtain a complete overview of the produced hydrogen bubble diameters.

6 Discussion

One of the main reasons for using LMS over regular backlighting is to decrease the defocus bias error which can reach up to 20% in the current experimental set-up. However, other criteria can also be used to avoid sizing out-of-focus bubbles as e.g. setting a threshold on the minimum acceptable magnitude of the shadow edge gradient. Nevertheless, these criteria are not rigorous and should be carefully calibrated for every set-up and bubble size (Honkanen et al. (2005)) to investigate the corresponding measurement volume (and defocus bias error). In addition, due to limitations imposed by the depth-of-field of each camera, these criteria are not able to select an arbitrarily small measurement volume and hence, one cannot limit the defocus bias error to a given target uncertainty. Indeed, even when a bubble is in-focus, its size can change because the optical magnification of the camera changes with the distance to the bubble (except when telecentric objectives are used). In the shown examples, this optical magnification change is superimposed with the out-of-focus blurring to create the stated sizing errors for bubbles drifting away from their in-focus location. In contrast, with LMS, the thickness of the laser-sheet can be set independently from the depth-of-field of the camera down to a thickness equal to the bubble diameter. This allows making the measurement volume smaller than the depth-of-field of the camera and

can decrease the optical magnification variations over the measurement volume (and its associated error). In addition, this also offers a larger flexibility in setting the measurement volume and does not require a tedious calibration for each image processing threshold.

Comparing LMS with the implementation of Haines and Johnson (1995), it is noted that the precise location of the glare points in the shadow contour is not taken into account. Thus, also glare points coming from multiple reflections of the laser could be seen as evidence that the bubble is inside the laser-sheet. As this is not necessarily the case, some out-of-focus bubbles might be sized. However, with LMS, a confined search for glare points as described in section 3 can be performed. This confined search will rule out many glare points coming from multiple reflections and will hence decrease the defocus bias errors more efficiently. Also, the precision of the spherical bubble/droplet diameter measurements is improved by an order of magnitude as the glare points are used to size the bubble/droplet and not the shadow contour diameter. Next to these two advantages of LMS, the main advantage of the approach of Haines and Johnson (1995) remains that the bubbles under investigation do not have to be spherical.

Interferometric Particle Imaging or IPI (Koenig et al. (1986); Glover et al. (1995); Maeda et al. (2002); Grassmann and Peters (2004)) can be used for measuring bubbles under 90° as was described in Dehaeck and van Beeck (2007a), Dehaeck and van Beeck (2007b) and in Kawaguchi and Maeda (2005). Such measurements also have a well-defined measurement volume, which is similarly displaced and dependent on the bubble diameter in the case of a Gaussian intensity profile of the laser-sheet. The main advantage of IPI is its capability of measuring microscopic bubbles with a regular objective, thus maintaining a field of view of several centimeters whereas LMS is limited to a field of view of 2 mm in the present case while using an expensive high magnification lens. In contrast, LMS typically is able to measure in flows with maximum void fractions (comparable to those of regular backlighting) that are up to an order of magnitude higher than those of IPI (Dehaeck et al. (2005)). Velocity measurements with LMS are also expected to be more accurate as such measurements are virtually identical to PTV measurements of which the uncertainty has been studied in several articles (e.g. Marxen et al. (2000)). This is due to a better localisation accuracy offered by the Gaussian peaks as compared to the diffuse out-of-focus discs. Finally, LMS is a more robust technique due to the redundancy offered by the combination of backlighting with GPVS. In IPI measurements, no redundancy is typically present (except for the set-up introduced in Dehaeck and van Beeck (2007b)) and fringe patterns arising from spuriously reflected glare points or overlapping out-of-focus discs can lead to misinterpretations.

Finally, experiments carried out in a dedicated electrochemical reactor have demonstrated that LMS is a robust technique capable of studying two-phase flows consisting of microbubbles. This showed that the detected bubble size and the flow field are tightly linked. As a result, for quantitative studies, the positioning of the field-of-view needs to be

done very accurately and should cover a substantial area in order to obtain a good spatial understanding of the bubble size distribution in the electrochemical reactor.

7 Conclusions

A combination of backlighting and GPVS was introduced called Laser Marked Shadowgraphy (LMS) which allows for an automated bubble sizing algorithm. LMS is a 2D optical measurement technique capable of sizing spherical bubbles, droplets and particles with a better accuracy compared to standard backlighting. Experiments showed that the error of standard backlighting could reach up to 20% due to the measurement of out-of-focus bubbles in our set-up, whereas LMS limited this error to 1%. Preliminary estimates show that the precision of LMS is about an order of magnitude higher than that of regular backlighting due to the use of a Gaussian interpolation of sharp intensity peaks. Compared to GPVS, LMS has a more robust image processing algorithm because the signature of a bubble is stronger. Finally, experiments were performed in an electrochemical reactor and the influence of the rotational speed on the bubble size distribution directly above the electrode was shown.

References

Albrecht, H.-E., Borys, M., Damaschke, N., and Tropea, C. (2003). *Laser Doppler and Phase Doppler Measurement Techniques*. Springer-Verlag.

Boissonneau, P. and Byrne, P. (2000). An experimental investigation of bubble-induced free convection in a small electrochemical cell. *Journal of Applied Electrochemistry*, 30:767–775.

Bongiovanni, C., Chevaillier, J. P., and Fabre, J. (1997). Sizing of bubbles by incoherent imaging: defocus bias. *Experiments in Fluids*, 23:209–216.

Dehaeck, S. and van Beeck, J. (2007a). Designing a maximum precision interferometric particle imaging set-up. *Experiments in fluids*, 42(5):767–781.

Dehaeck, S. and van Beeck, J. (2007b). Multi-frequency interferometric particle imaging for bubbly flows. *Experiments in fluids*.

Dehaeck, S., van Beeck, J. P. A. J., and Riethmuller, M. L. (2005). Extended glare point velocimetry and sizing for bubbly flows. *Experiments in fluids*, 39(2):407–419.

Glover, A., Skippon, S., and Boyle, R. (1995). Interferometric laser imaging for droplet sizing: a method for droplet-size measurement in sparse spray systems. *Applied Optics*, 34:8409–8421.

Grassmann, A. and Peters, F. (2004). Size measurement of very small spherical particles by mie scattering imaging (MSI). *Part. Part. Syst. Charact.*, 21:379–389.

Haines, M. and Johnson, B. (1995). Injected bubble populations in seawater and fresh water measured by a photographic method. *Journal of geophysical research (Oceans)*, 100(C4):7057–7068.

Honkanen, M., Saarenrinne, P., Stoor, T., and Niinimäki, J. (2005). Recognition of highly overlapping ellipse-like bubble images. *Meas. Sci. Technol.*, 16(9):1760–1770.

Kawaguchi, T. and Maeda, M. (2005). Measurement technique for analysis in two-phase flows involving distributed size of droplets and bubbles using interferometric method - planar simultaneous measurement of size and velocity vector field. *Multiphase Science and Technology*, 17(1-2):57–77.

Koenig, G., Anders, K., and Frohn, A. (1986). A new light-scattering technique to measure the diameter of periodically generated moving droplets. *Journal of Aerosol Sciences*, 17:157–167.

Lindken, R. and Merzkirch, W. (2002). A novel PIV technique for measurements in multiphase flows and its applications to two-phase flows. *Experiments in Fluids*, 33:814–825.

Maeda, M., Akasaka, Y., and Kawaguchi, T. (2002). Improvements of the interferometric technique for simultaneous measurement of droplet size and velocity vector field and its application to a transient spray. *Experiments in Fluids*, 33:125–134.

Marxen, M., Sullivan, P. E., Loewen, M. R., and Jaehne, B. (2000). Comparison of gaussian particle center estimators and the achievable measurement density for particle tracking velocimetry. *Experiments in Fluids*, 29:145–153.

Minor, L. and Sklansky, J. (1981). Detection and segmentation of blobs in infrared images. In *IEEE Trans. SMC 11*, pages 194–201.

Pla, F. (1996). Recognition of partial circular shapes from segmented contours. *Computer vision and image understanding*, 63(2):334–343.

Rad, A., Faez, K., and Qaragozlou, N. (2003). Fast circle detection using gradient pair vectors. In Sun, C., Talbot, H., Ourselin, S., and Adriaansen, T., editors, *Proc. VIIth Digital Image Computing: Techniques and Applications*.

Ren, K., Lebrun, D., Ozkul, C., Kleitz, A., Gouesbet, G., and Grehan, G. (1996). On the measurements of particles by imaging methods: theoretical and experimental aspects. *Part. Part. Syst. Charact.*, 13:156–164.

Van Parys, H., Tourwé, E., Depauw, M., Breugelmans, T., Deconinck, J., and Hubin, A. (2007). IRDE and RDE electrochemical cells evaluation: comparison of electron and mass transfer. In *Simulation of electrochemical processes II, ELECTROCOR 2007,WIT press*.

Wedin, R., Davoust, L., Cartellier, A., and Byrne, P. (2003). Experiments and modelling on electrochemically generated bubbly flows. *Experimental Thermal and Fluid Science*, 27(6):685–696.